# Restricted-Geometry Quantum Models Beyond Atoms: Application to NSDI in Diatomic Systems

Lars C. Bannow, Jan H. Thiede, Michał Ogryzek, Dmitry K. Efimov, and Jakub S. Prauzner-Bechcicki<sup>3,\*</sup>

<sup>1</sup>Fachbereich Physik, Philipps-Universität Marburg, D-35032 Marburg, Germany
 <sup>2</sup>Institute of Theoretical Physics, Faculty of Fundamental Problems of Technology,
 Wrocław University of Science and Technology, 50-370 Wrocław, Poland
 <sup>3</sup>Jagiellonian University in Kraków, Faculty of Physics, Astronomy and Applied Computer Science,
 Marian Smoluchowski Institute of Physics, Lojasiewicza 11, 30-348 Krakow, Poland
 (Dated: November 10, 2025)

We present a (1+1)-dimensional quantum model designed to describe nonsequential double ionization (NSDI) in homonuclear diatomic molecules exposed to strong linearly polarized laser fields. Extending the restricted-geometry framework previously developed for atomic systems, our approach captures key features of NSDI, including the characteristic knee structure in double ionization yields. Despite its simplifying assumptions, the model shows good agreement with experimental data and proves particularly suitable for systems with  $\sigma$ -type orbital symmetry. It offers a computationally efficient tool for exploring multi-electron dynamics in molecular systems.

#### I. INTRODUCTION

Experimental observations of strong-field phenomena such as above-threshold ionization (ATI), high-harmonic generation (HHG), and non-sequential ionization (NSI) have posed significant challenges for theoretical interpretation. While acknowledging the many efforts and diverse approaches, it seems justified to state that breakthroughs in our understanding of these processes have often come from simple models that offered intuitive explanations and indicated where new phenomena might be expected. A prominent example is the single active electron (SAE) approach, followed by the strong-field approximation (SFA), which significantly advanced in particular the theoretical description of HHG, NSI, and other strong-field phenomena [1, 2]. Interestingly, this highly successful method was preceded by an even simpler classical concept, the so-called simple-man model, also known as the rescattering scenario [3, 4].

Building on this foundational model, Eckhardt and Sacha proposed a new perspective on non-sequential double ionization (NSDI) of atoms [5-10], which led to the introduction of a novel restricted-geometry quantum model [11, 12]. This model successfully reproduced and explained key experimental observations, such as the knee structure in the ionization yield curve [13-16], the double-hump structure in the ion momentum distribution [17, 18], and characteristic structures in two-electron momentum distributions [19-21], while also enabling the analysis of NSDI across a broad range of laser field parameters [22-27].

The approach was subsequently compared to other restricted-geometry concepts [28] and later extended to describe triple ionization [28–35]. In this work, we further advance the restricted-geometry quantum framework, originally proposed by Eckhardt and Sacha, to ex-

plore its predictive power and limitations in describing multi-electron dynamics under strong laser fields. Particular emphasis is placed on the mechanisms of non-sequential and sequential ionization processes in diatomic molecules.

Available data for diatomic and other small molecules clearly exhibit signatures of non-sequential double ionization (NSDI) similar to those observed in atoms, while also revealing important differences [36–69]. These differences stem from the richer internal structure of molecules compared to atoms and the presence of additional degrees of freedom, such as the existence of a molecular axis. They manifest as suppressed ionization yields, modified momentum distributions, and angular dependencies; for example, sensitivity to the alignment between the molecular axis and the laser polarization direction.

The double ionization of diatomic molecules has been actively studied over the past 25 years. Experimentally, the double ionization yield has been investigated in  $H_2$  and  $D_2$  as a function of laser field polarization [40], and in  $O_2$  and  $N_2$  with respect to orbital configuration [41]. Studies on heteronuclear diatomic molecules have focused on the role of multiorbital contributions [61], and were later extended to polyatomic systems in linearly polarized fields, with particular attention to NSDI efficiency [62]. Other experiments have targeted subcycle resolution of  $H_2$  ionization [63] and the analysis of momentum distributions following double ionization of homonuclear molecules [43, 66].

In parallel, a wide range of theoretical and numerical methods have been developed to interpret these findings. Classical trajectory simulations have been extensively used to study the double ionization knee [48, 58], with some approaches incorporating tunneling of the first electron via ADK-based initial conditions [45, 55], while others relied on purely classical dynamics [50, 52]. Analytical S-matrix methods have also been applied to explore alignment-dependent effects [49, 57].

Quantum models, including one-dimensional and

<sup>\*</sup> jakub.prauzner-bechcicki@uj.edu.pl

cylindrical (3D for two electrons) approaches, have enabled the study of ionization channels and alignment effects [47]. The introduction of a four-dimensional model (two spatial dimensions per electron) [59] allowed for the investigation of two-center interference in molecular double ionization. More recently, a density-matrix-based semi-analytical framework has been proposed to describe sequential double ionization in molecules [67–69].

It is evident that models developed for atomic systems fall short in capturing the molecular-specific effects. To address this, theoretical approaches must be adapted or extended to incorporate parameters such as internuclear separation and orientation-dependent ionization pathways. In this work, we aim to extend the restricted-geometry quantum framework to diatomic molecules and assess its ability to capture both universal and molecule-specific features of strong-field ionization. Our findings aim to contribute to a more unified understanding of multi-electron dynamics in atoms and molecules under intense laser fields.

The paper is organized as follows. In Section II, we discuss the rationale behind the restriction of geometry. Section III briefly outlines the numerical approach. In Section IV, we present and analyze the ionization yields and momentum distributions. Finally, conclusions are drawn in Section V. Atomic units are used throughout the paper unless stated otherwise.

# II. RATIONALE FOR RESTRICTED GEOMETRY

We consider atoms or molecules interacting with a strong, short, linearly polarized laser pulse. The z-axis is the polarization axis. Below, we provide a concise overview of the approach that enables dimensionality reduction in the case of atoms. A more detailed discussion can be found in previous papers [5-12].

Nowadays, the rescattering scenario [3, 4] is widely accepted as the underlying mechanism of NSDI. In this three-step process, electrons assist each other in escaping the atomic or molecular potential. In the first step, one electron escapes near a field maximum via tunneling or over-the-barrier ionization. It is then accelerated by the laser field and driven back towards the core when the field reverses its sign. Upon recollision, the second electron may be released either immediately (so-called direct ionization) or after a delay, following excitation by the first electron and subsequent field ionization (recollision-induced excitation with subsequent ionization, RESI). Other mechanisms are also possible, such as the sling-shot scenario [70] or multiple recollision cycles.

The last step of the rescattering scenario can also be viewed from a slightly different, adiabatic perspective. Upon interaction with the ion and the second electron remaining near the core, the returning electron may become "captured," forming a doubly excited complex [25, 71]. The quotation marks emphasize that this

complex is typically interpreted either as a virtual intermediate state or as a real, short-lived transient Coulomb complex. In this picture, the observed effects of rescattering are understood as decay channels of this transient state, leading to various outcomes: simultaneous ionization of both electrons (direct ionization), delayed ionization (RESI), or even purely sequential double ionization.

Decay channels of the transient state can be identified through a local stability analysis of the adiabatic full-dimensional potential [72]. This approach has been successfully applied to the study of NSDI in atoms [5–10], leading to a key observation: simultaneous escape of both electrons, responsible for signatures of correlated motion visible in ion momentum distributions and two-electron momentum maps, is possible only in the vicinity of a specific subspace. In this subspace, the electrons move symmetrically with respect to the laser polarization axis and pass sufficiently close to saddle points formed by the interplay between Coulomb interactions and the external electric field. These saddles act as gateways for correlated ionization, and their geometry and accessibility strongly influence the likelihood of direct double ionization.

In the case of atoms, the analysis of saddle points has shown that their position depends on both the field amplitude and the number of active electrons considered. While the former determines the distance between the saddle and the nucleus, the latter constrains the motion of the saddle in configuration space. When visualized in three-dimensional space, the saddle lies on a straight line inclined at a constant angle of  $\alpha = \pm \pi/6$  with respect to the laser polarization axis, at a distance from the nucleus  $r_s$  with (see [7])

$$r_s^2 = \frac{\sqrt{3}}{|F(t)|},\tag{1}$$

where F(t) is the instantaneous electric field amplitude at time t. Thus, the position of the saddle in cylindrical coordinates is given by (see [7])

$$\begin{cases} Z_S = r_s \cos \alpha \\ R_S = r_s \sin \alpha \end{cases} , \tag{2}$$

as illustrated in Fig. 1 of that reference. Since the saddle acts as a gateway for the correlated escape of electrons, their motion can be effectively confined to two lines defined by Eq. (2), resulting in a (1+1)-dimensional model atom [11, 12].

A first extension of the above approach to diatomic homonuclear molecules was presented in [73, 74], where the saddles of the adiabatic full-dimensional potential were analyzed, the symmetric  $C_{2v}$  subspaces were identified, and classical simulations of the decay process were performed, yielding ion momentum and two-electron momentum distributions for  $N_2$  and  $O_2$  molecules. In the present work, we extend this analysis by developing a fully quantum model. But before proceeding, we briefly recap the structure of the identified subspaces and the properties of the corresponding saddle points.

# A. Symmetric subspaces and saddle structure

Since the proposed model for diatomic homonuclear molecules is an extension of the approach successfully applied to atomic systems, we will use the atomic case (referred to as the helium atom) as a benchmark. Throughout this analysis, we neglect nuclear motion by assuming that the nuclei are infinitely heavy compared to the electrons. The starting point is a hydrogen-like Hamiltonian of the form

$$H = \frac{\mathbf{p}_1^2}{2} + \frac{\mathbf{p}_2^2}{2} + V,\tag{3}$$

where  $\mathbf{p}_i$  denotes the momentum of the *i*-th electron, and V is the total potential consisting of two parts:

$$V = V_C + V_I, (4)$$

here, we denote the Coulomb term by  $V_C$  and the field interaction term by  $V_I$ , respectively. The field interaction term is similar for both helium and the molecule. Using the dipole approximation and assuming a linearly polarized laser field F(t) along the z-axis, it takes the form

$$V_I = (z_1 + z_2)F(t). (5)$$

The Coulomb term, on the other hand, distinguishes helium from molecular systems. Specifically, for helium it reads

$$V_C^{He} = -\sum_{i=1}^2 \frac{2}{r_i} + \frac{1}{|\mathbf{r}_1 - \mathbf{r}_2|},$$
 (6)

whereas for a diatomic molecule it is given by

$$V_C^M = -\sum_{i=1}^2 \frac{1}{\sqrt{(x_i + \frac{d}{2}\sin\theta)^2 + y_i^2 + (z_i + \frac{d}{2}\cos\theta)^2}}$$
$$-\sum_{i=1}^2 \frac{1}{\sqrt{(x_i - \frac{d}{2}\sin\theta)^2 + y_i^2 + (z_i - \frac{d}{2}\cos\theta)^2}}$$
$$+\frac{1}{|\mathbf{r}_1 - \mathbf{r}_2|}.$$
 (7)

Here, the center of mass of the nuclei is placed at the origin of the coordinate system and d is the distance between the nuclei. Without loss of generality, the nuclei are assumed to lie in the xz-plane, and  $\theta$  denotes the angle between the molecular axis and the laser polarization axis. In both cases,  $\mathbf{r}_i = (x_i, y_i, z_i)$  denotes the position of the i-th electron.

Local analysis of the adiabatic potential, Eq. (4), with the molecular Coulomb term given by Eq. (7), allowed Prauzner-Bechcicki *et al.* to identify three two-dimensional,  $C_{2v}$ -symmetric subspaces (see [73] for details). These configurations are illustrated in Fig. 1.

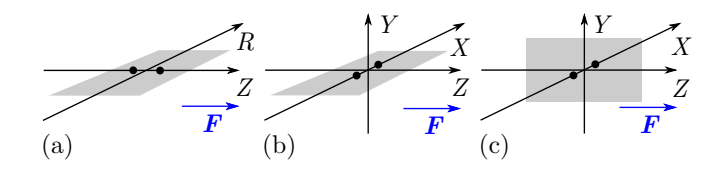


FIG. 1. (Color online) The three configurations leading to the model potentials  $V_{\parallel}$  (a),  $V_{\perp 2}$  (b), and  $V_{\perp 3}$  (c). Black dots represent the protons, the gray shaded plane indicates the plane in which the electrons move, and  $\boldsymbol{F}$  denotes the field polarization axis, which is aligned with the Z-axis in all cases. In panel (c), one proton is located in front of the gray plane, and the other behind it.

In the first configuration, the molecular axis is aligned with the field polarization axis, i.e.,  $\theta = 0$  (Fig. 1(a)). Since this is a parallel alignment, we denote the corresponding potential by  $V_{\parallel}$ , which includes both Coulomb and interaction terms. Introducing cylindrical coordinates due to the axial symmetry of the configuration and restricting the electrons to symmetric motion in a plane (i.e.,  $r_i = R$ ,  $\varphi_1 - \varphi_2 = \pi$ ,  $z_i = Z$ ), we obtain

$$V_{\parallel}(R,Z,t) = -\frac{2}{\sqrt{R^2 + (Z+d/2)^2}} - \frac{2}{\sqrt{R^2 + (Z-d/2)^2}} + \frac{1}{2|R|} + 2ZF(t).$$
 (8)

The second configuration corresponds to the case where the molecular axis lies in the XZ-plane and is perpendicular to the field polarization direction, i.e.,  $\theta=\pi/2$ . The electrons are restricted to symmetric motion in the XZ-plane (Fig. 1(b)). The resulting potential is

$$V_{\perp 2}(X, Z, t) = -\frac{2}{\sqrt{Z^2 + (X + d/2)^2}} - \frac{2}{\sqrt{Z^2 + (X - d/2)^2}} + \frac{1}{2|X|} + 2ZF(t).$$
(9)

We denote this configuration by  $V_{\perp 2}$ , as the molecular axis and the field polarization axis are *perpendicular*, and the electrons move in the plane spanned by both axes. All components of the model are thus confined to a two-dimensional plane.

Finally, we consider the case where the molecular axis is again *perpendicular* to the field polarization axis  $(\theta = \pi/2)$ , but the electrons are restricted to symmetric motion in the YZ-plane, while the nuclei remain in the XZ-plane (Fig. 1(c)). Although the dynamics take place in the YZ-plane, the configuration is "quasi" three-dimensional, and we denote the potential by

$$V_{\perp 3}(Y, Z, t) = -\frac{4}{\sqrt{Y^2 + Z^2 + d^2/4}} + \frac{1}{2|Y|} + 2ZF(t).$$
(10)

# Restricted-Geometry Hamiltonian

Sacha and Eckhardt suggested in [6, 7] that correlated double ionization requires the electrons to escape simultaneously, crossing a pair of saddles formed by the interplay between nuclear attraction, interaction with the electric field, and electron-electron repulsion. Naturally, in the molecular case, the three two-dimensional potentials (8), (9), and (10) exhibit saddles located at different positions and with different properties, which may affect the ionization signals.

For the helium atom, Eckhardt and Sacha showed that the saddles lie along two straight lines inclined at an angle of  $\alpha = \pm \pi/6$  with respect to the z-axis, independent of the field strength F [6, 7]. This allows for a coordinate transformation that restricts the electron motion to these lines [10]. In contrast, for molecules, the simple scaling symmetry of the atomic case is lost, and the saddle positions can no longer be parametrized by straight lines.

Figure 2 shows the saddle positions (blue circles) for various field strengths and for the three molecular configurations. For comparison, the straight lines corresponding to the helium atom placed at the origin are also shown. At low field strengths, the saddles are located far from the molecule and approximately follow these straight lines. However, at higher field strengths, the saddles move closer to the nuclei and deviate from the straight-line paths. To quantify this deviation, we define

$$\delta = \frac{|x_s^{\text{Mol}} - x_s^{\text{He}}|}{2\max(|x_s^{\text{Mol}}|, |x_s^{\text{He}}|)},\tag{11}$$

where  $x_s^{\text{Mol}}$  is the R, X or Y coordinate of the saddle in the molecular case (depending on the configuration), and  $x_s^{\text{He}}$  is the corresponding coordinate for helium. Using internuclear distances for N2, O2 and S2 (see Table I) and peak field amplitudes of F = 0.22 a.u. for  $N_2$ , F = 0.16 a.u. for  $O_2$ , and F = 0.12 a.u. for  $S_2$ , we find that the maximum deviations fall within the range  $\delta = (8.6 \pm 4.0) \%$ . Thus, the straight-line approximation still provides a reasonable representation of the saddle trajectories, as originally proposed in [6].

For the configurations represented by  $V_{\parallel}$  (Eq. (8), Fig. 1(a)) and  $V_{\perp 2}$  (Eq. (9), Fig. 1(b)), we apply the coordinate transformation  $x_i = (-1)^i r_i/2$ ,  $z_i = \sqrt{3}r_i/2$ , and  $y_i = 0$  for i = 1, 2 [10], in Eqs. (5) and (7). In the third configuration, represented by  $V_{\perp 3}$  (Eq. (10), Fig. 1(c)), the roles of  $x_i$  and  $y_i$  are interchanged. For notational compactness, we define the set  $\mathcal{R} = \{r_1, -r_1, r_2, -r_2\},\$ and in the expressions below,  $r \in \mathcal{R}$  indicates that the potential is computed as a sum over all values in this set.

The electron-core interaction terms  $\widetilde{V}$  for the three

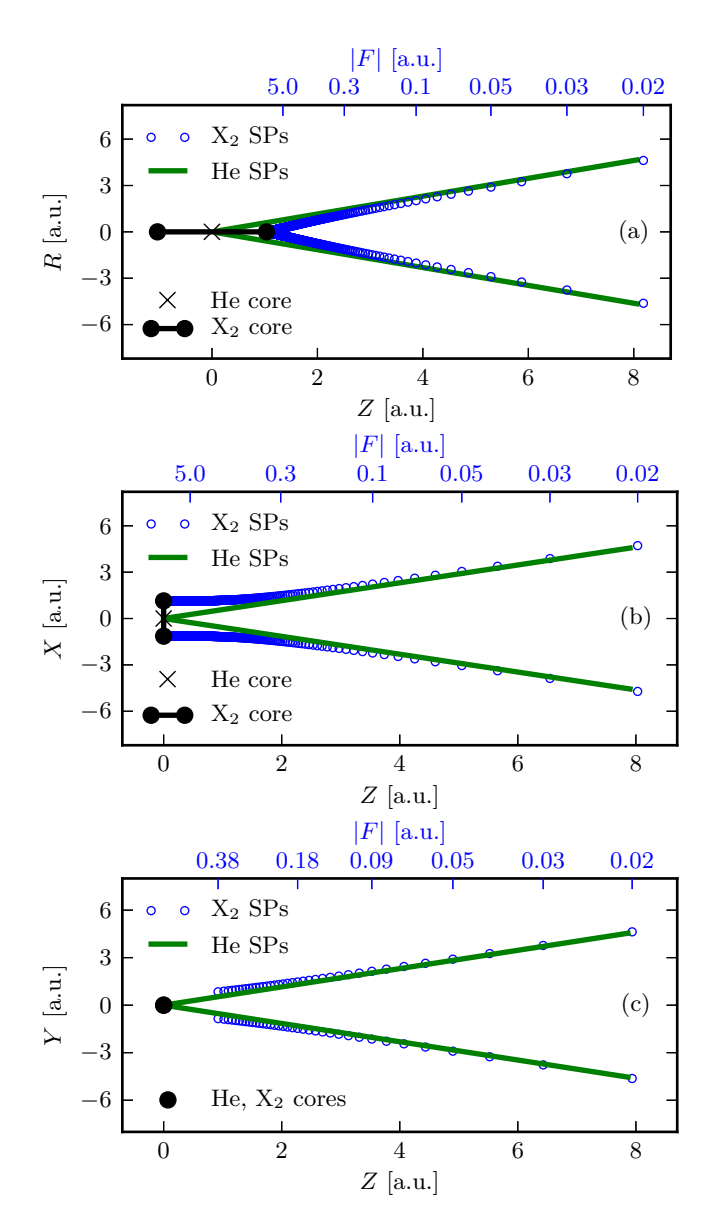


FIG. 2. (Color online) The saddle points (SPs) of the model potentials  $V_{\parallel}$  (a),  $V_{\perp 2}$  (b), and  $V_{\perp 3}$  (c) for a diatomic molecule  $X_2$  with internuclear distance d = 2.28 a.u. are shown in blue. For comparison, saddle points for the helium atom are shown in green. In the case of  $V \perp 3$ , solutions exist only for field amplitudes |F| < 0.39 a.u. The upper axis displays the absolute peak field amplitude |F| corresponding to the molecular saddle positions.

configurations are then given by

$$\widetilde{V}_{\parallel}(r_1, r_2) = -\sum_{r \in \mathcal{R}} \frac{1}{\sqrt{r^2 + rd\sqrt{3}/2 + d^2/4}}, (12)$$

$$\widetilde{V}_{\perp 2}(r_1, r_2) = -\sum_{r \in \mathcal{R}} \frac{1}{\sqrt{r^2 + rd/2 + d^2/4}}, \qquad (13)$$

$$\widetilde{V}_{\perp 3}(r_1, r_2) = -\frac{2}{\sqrt{r_1^2 + d^2/4}} - \frac{2}{\sqrt{r_2^2 + d^2/4}}. \qquad (14)$$

$$\widetilde{V}_{\perp 3}(r_1, r_2) = -\frac{2}{\sqrt{r_1^2 + d^2/4}} - \frac{2}{\sqrt{r_2^2 + d^2/4}}.$$
 (14)

The electron–electron repulsion and field interaction terms are identical for all three configurations

$$V_{12}(r_1, r_2) = \frac{1}{\sqrt{(r_1 - r_2)^2 + r_1 r_2}}, \tag{15}$$

$$V_I(r_1, r_2, t) = \frac{\sqrt{3}}{2} F(t)(r_1 + r_2).$$
 (16)

The resulting Hamiltonian for the restricted-geometry model reads

$$H = \frac{p_1^2 + p_2^2}{2} + \widetilde{V} + V_{12} + V_I, \tag{17}$$

where  $\widetilde{V}$  is the only term that distinguishes between the three configurations.

## C. Model Assumptions and Limitations

Since our aim in this work is to explore the predictive power and limitations of the restricted-geometry quantum framework as applied to NSDI in diatomic molecules, a few comments are in order before we proceed to the numerical implementation and discussion of the results.

First, we note that the starting point of our approach is a hydrogen-like Hamiltonian. At this level, the internal structure of the target (atom or molecule) is not explicitly included, similar to the SAE approximation commonly used in the description of HHG or ATI. Regardless of the atomic species, SAE assumes that only one electron interacts with the field, while the influence of the remaining electrons is incorporated into an effective potential. In our case, we include two active electrons, and the only parameter in the Hamiltonian that reflects the molecular species is the internuclear distance d. In this sense, the model describes hydrogen-molecule-like systems. However, in the numerical implementation (see next section), we also introduce a parameter that allows us to set the ionization potential, thereby tailoring the model to a specific molecular species.

An open question remains: to what extent can molecular symmetries, such as the distinction between  $\sigma$  and  $\pi$  orbitals, be mapped onto the initial wave function within the restricted-geometry quantum framework? Similar considerations have been made in the context of differences between the ground and excited states of helium [23], as well as in studies of triple ionization [29–34]. This issue may serve as a fruitful direction for future research, particularly in the context of extending the model to more complex molecular systems.

Second, the simplified model includes only two orientations of the molecule with respect to the laser polarization axis. This limits the ability to analyze ionization for randomly oriented molecules; averaging over just two orientations is not meaningful. Nevertheless, the two considered orientations, parallel and perpendicular, are experimentally accessible and relevant.

Third, nuclear motion and its influence on ionization channels are neglected in the present approach. At this stage, there appears to be no straightforward way to incorporate this degree of freedom within the current framework.

Fourth, an extension of the approach to triple and higher-order ionization is, in principle, possible. Such generalizations would follow similar lines to those developed for atomic systems [29, 32, 33].

Finally, extending the framework beyond diatomic molecules is conceivable. However, in such cases, molecular symmetries are expected to play a much more significant role and would likely require a more elaborate treatment.

#### III. NUMERICAL APPROACH

The first obstacle in the numerical implementation of the proposed model is the presence of singularities in the Coulomb terms. To eliminate these singularities, we introduce a cut-off parameter  $\epsilon>0$  such that

$$\frac{1}{\sqrt{f(r_1, r_2, d)}} \longrightarrow \frac{1}{\sqrt{f(r_1, r_2, d) + \epsilon}}.$$
 (18)

This standard smoothing procedure [11, 29, 35, 75–81] allows us to regularize the Coulomb singularities. Both  $\epsilon$  and the internuclear distance d can be used to tune the spectrum of the Hamiltonian (17), enabling us to approximate the ionization energies of real molecules. In our approach, we take d from experimental data and vary only  $\epsilon$  (see Table I).

In the following, we consider three diatomic molecules: N<sub>2</sub> (d=2.07 a.u.), O<sub>2</sub> (d=2.28 a.u.), and S<sub>2</sub> (d=3.57 a.u.). For each potential ( $V_{\parallel}$ ,  $V_{\perp 2}$ , and  $V_{\perp 3}$ ), an appropriate value of  $\epsilon$  is determined numerically by solving the field-free time-dependent Schrödinger equation in imaginary time [76], both for the neutral molecule (using the full Hamiltonian (17)) and for the corresponding molecular ion (by taking the limit  $r_2 \to \infty$  in (17)). The resulting ionization energies are then compared to experimental values.

Each model molecule is thus characterized by an internuclear distance d and three cut-off parameters  $\epsilon$ , one for each potential configuration. These values, along with the corresponding ionization energies, are listed in Table I. We find that it is always possible to obtain a good approximation to the experimental ionization energies, although the different subspaces require different values of  $\epsilon$ .

The time-dependent Schrödinger equation is solved on an  $L \times L$  square grid using the split-operator technique combined with the fast Fourier transform (FFT) algorithm [84, 85]. The grid size L is first adjusted during the imaginary-time propagation to ensure proper convergence of the ground state. Once the system is exposed to the laser pulse, the grid is extended to accommodate

		$V_{\parallel}$	$V_{\perp 2}$	$V_{\perp 3}$
$N_2$ : $d = 2.07$ a.u.	exp.	$\epsilon = 1.6$	$\epsilon = 1.2$	$\epsilon = 1.1$
$E_g$ [eV]	-42.7	-42.0	-41.9	-41.1
$E_a^+$ [eV]	-27.1	-28.1	-28.8	-28.7
$E_I^+$ [eV]	15.6	13.9	13.1	12.4
$O_2$ : $d = 2.28$ a.u.	exp.	$\epsilon = 2.3$	$\epsilon = 1.9$	$\epsilon = 1.6$
$E_g$ [eV]	-36.2	-36.1	-36.0	-36.3
$E_q^+$ [eV]	-24.1	-24.3	-24.6	-25.2
$E_I^+$ [eV]	12.1	11.8	11.4	11.1
$S_2$ : $d = 3.57$ a.u.	exp.	$\epsilon = 2.7$	$\epsilon = 1.3$	$\epsilon = 1.2$
$E_g$ [eV]	-28.1	-29.8	-30.0	-28.4
$E_q^+$ [eV]	$-18.7^{\rm a}$	-20.1	-21.5	-20.9
$E_I^+$ [eV]	9.4	9.7	8.5	7.5

<sup>&</sup>lt;sup>a</sup> For  $S_2$ , no experimental value of  $E_g^+$  could be found in the literature. The value listed in the table was estimated by assuming that the ratio of ground-state to ionic-state ionization energies is the same as for  $O_2$ , i.e.,  $E_q^+(S_2)$  was approximated as  $E_I^+(S_2) \times E_g^+(O_2)/E_I^+(O_2)$ . This approximation is used solely for the purpose of parameter tuning and does not affect the generality of the model.

TABLE I. Ground state energies of the neutral molecule  $(E_q)$ , ground state energies of the singly ionized molecule  $(E_q^+)$  and first ionization energies  $(E_I^+ = E_g^+ - E_g)$  for the model versions of N<sub>2</sub>, O<sub>2</sub> and S<sub>2</sub>, compared to the experimental (exp.) energies of the real molecules [82, 83]. The origin of the energy axis is the ground state energy of the doubly ionized molecule,  $E_g^{2+} = 0$  eV.

rescattered electrons. Specifically, the grid size is chosen to satisfy the condition  $L \gg 2|F|/\omega^2$ , i.e., it significantly exceeds the classical quiver distance. The extension is performed while keeping the grid-point density constant. To prevent spurious reflections of the wave function at the grid boundaries, absorbing boundary conditions are applied.

To calculate the ionization yield, we follow the method used in the atomic case [11, 12, 86]. The configuration space is divided into three types of regions:

- region M, corresponding to the neutral molecule,
- regions  $S_i$ , corresponding to singly ionized molecule,
- and regions  $D_i$ , corresponding to doubly ionized

with i = 1, ..., 4. This division is based solely on geometric criteria:

- if  $|r_1| > 8$  a.u. and  $|r_2| > 8$  a.u., the wave function is in one of the  $D_i$  regions;
- if  $(|r_1| > 14 \text{ a.u. and } |r_2| < 8 \text{ a.u.})$  or  $(|r_1| < 8 \text{ a.u.})$ and  $|r_2| > 14$  a.u.), it is in one of the  $S_i$  regions;
- otherwise, it is in the M region.

The ionization yield is then calculated as the probability flux between these regions. The detailed procedure is analogous to that described in [12].

To obtain momentum distributions, we follow the method proposed by Lein et al. [80] and later applied to studies of double [12] and triple ionization in atoms [33]. The whole configuration space is divided into four regions:

- $M_{\text{in}}$  ( $|r_1|, |r_2| < a$ ),
- $M_1$  ( $|r_1| > a$ ,  $|r_2| < a$ ),
- $M_2$  ( $|r_1| < a$ ,  $|r_2| \ge a$ ),
- and  $M_{\text{out}}$   $(|r_1|, |r_2| \ge a)$ .

The parameter a is chosen to exceed the classical quiver distance, ensuring that once an electron reaches this distance, it is unlikely to return. In region  $M_{\rm out}$ , Coulomb interactions are neglected, and the wave function is evolved in momentum space via multiplication by a phase factor. In regions  $M_1$  and  $M_2$ , the Coulomb interaction between electrons and the interaction with the nuclei for the more distant electron are neglected. In  $M_{\rm in}$ , the full Hamiltonian is used.

Wave function transfer between regions is performed using the "smooth cutting and coherent adding" procedure [80]. The two-electron momentum distribution is obtained by coherently collecting the wave function from all regions, while smoothly removing contributions corresponding to the neutral and singly ionized molecule. The modulus square of the resulting wave function in momentum space yields the two-electron momentum distribution. For a comprehensive description of the wave function transfer technique and the construction of twoelectron momentum distributions, we refer the reader to [12].

The ion momentum distribution is then obtained as the marginal distribution of the variable

$$p_{\parallel}^{2+} = -\frac{\sqrt{3}}{2}(p_1 + p_2). \tag{19}$$

Before moving on, we add one final comment. Both the actual molecules and the models described above differ in their ionization energies. A meaningful comparison between different cases can be based on an approximate classical scaling. Consider two molecules with groundstate energies E and E'. To relate the two, we introduce an effective quantum number  $q := \sqrt{E'/E}$  and consider the scaling of the classical Hamiltonian

$$H(q^{-2}r_i, qp_i, q^{-3}t, q^4F_0, q^3\omega, \phi, q^{-4}\epsilon, q^{-2}d) = q^2H(r_i, p_i, t, F_0, \omega, \phi, \epsilon, d)$$
(20)

This implies that the field parameters scale as

$$F'_0 = F_0 q^4,$$
 (21)  
 $\omega' = \omega q^3.$  (22)

$$\omega' = \omega q^3. \tag{22}$$

Molecule	$E_g$ [eV]	$\omega$ [a.u.]	$F_0$ [a.u.]
$\overline{\mathrm{N}_{2}}$	-42.0	0.075	0.22
$O_2$	-36.1	0.060	0.16
$S_2$	-29.8	0.045	0.11

TABLE II. Frequencies  $\omega$  and example peak field amplitudes  $F_0$  in a.u. that coincide with respect to classical scaling. We used the listed ground state energies  $E_g$  from potential  $V_{\parallel}$  (see Table I) and selected the O<sub>2</sub> frequency and peak field amplitude as reference values for rescaling to obtain the respective values for N<sub>2</sub> and S<sub>2</sub> listed above.

The scaling law (20) also suggests that the cut-off parameter  $\epsilon$  and the internuclear distance d can be mapped While perfect agreement cannot be exaccordingly. pected, since the ground-state energies are obtained from quantum mechanical calculations, the trend is consistent. For example, rescaling the  $O_2$  parameters to match  $N_2$ yields d = 1.96 a.u. and  $\epsilon = 1.7$   $(V_{\parallel}), \epsilon = 1.4$   $(V_{\perp 2}),$ and  $\epsilon = 1.2 \ (V_{\perp 3})$ , which compare reasonably well with the actual  $N_2$  values listed in Table I. In fact, d is slightly smaller and  $\epsilon$  slightly larger than the empirically adjusted values, so the deviations partially compensate. For  $S_2$ , however, the rescaled values deviate more significantly. Thus, while the scaling is not perfectly implemented, the discrepancies are comparable to those observed in the saddle-point positions.

In the next section we take advantage of the classical scaling of the field parameters to improve the comparability of ionization yields for the three molecular species  $N_2$ ,  $O_2$ , and  $S_2$ .

# IV. RESULTS

In this section, we discuss the results of propagating the ground-state wave functions for the three molecules  $N_2$ ,  $O_2$ , and  $S_2$ , using the three model potentials in the presence of a linearly polarized laser field derived in Sec. II. Results for the potential  $V_{\perp 3}$  are not shown, as they closely resemble those obtained for the other two configurations and do not reveal any additional features beyond what is already evident from the comparison between  $V_{\perp 2}$  and  $V_{\parallel}$ . Unless stated otherwise, all simulations are performed using the same laser pulse as in [25], consisting of  $n_c=5$  field cycles and a carrier-envelope phase  $\phi=0$ .

In the following subsections, we compare ionization yield curves for different molecular alignments and species, and present results for momentum distributions. We emphasize once again that the analysis of molecular alignment is limited to two extreme orientations, parallel and perpendicular, while the molecular species differ only in their internuclear distance and ionization energy. In the diagrams, ionization yields are color-coded for clarity and consistency across comparisons: red for  $N_2$ , blue for  $O_2$ , and yellow for  $S_2$ .

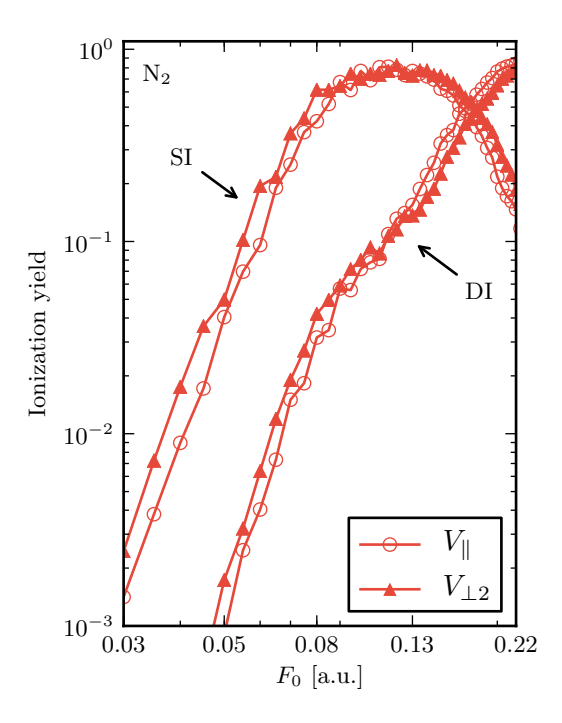


FIG. 3. (Color online) Single ionization (SI) and double ionization (DI) yield curves of potentials  $V_{\parallel}$  and  $V_{\perp 2}$  at a frequency of  $\omega = 0.075$  a.u. for N<sub>2</sub>.

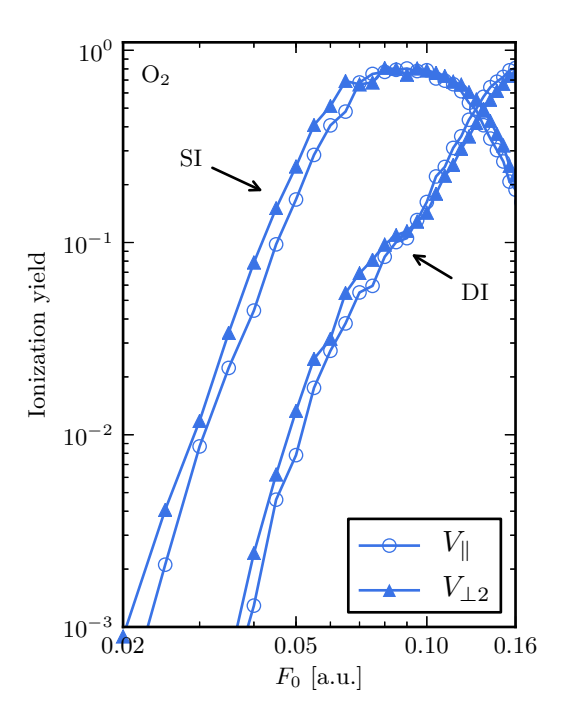


FIG. 4. (Color online) Single ionization (SI) and double ionization (DI) yield curves of potentials  $V_{\parallel}$  and  $V_{\perp 2}$  at a frequency of  $\omega = 0.06$  a.u. for  $O_2$ .

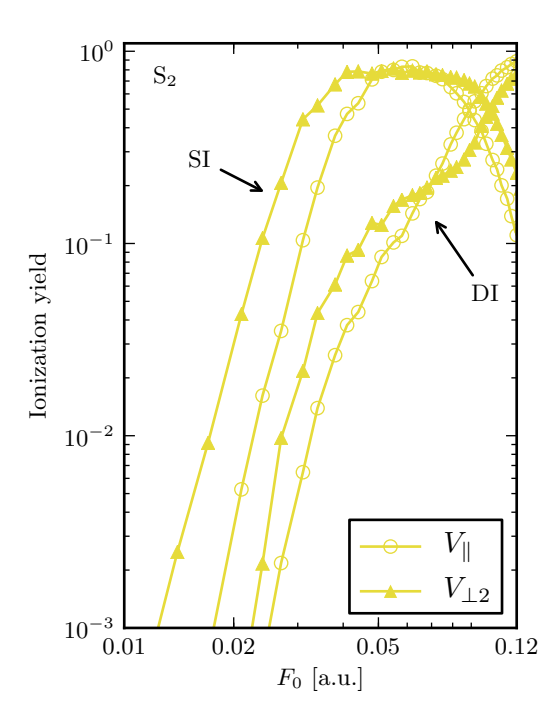


FIG. 5. (Color online) Single ionization (SI) and double ionization (DI) yield curves of potentials  $V_{\parallel}$  and  $V_{\perp 2}$  at a frequency of  $\omega = 0.045$  a.u. for  $S_2$ .

#### A. Ionization Yields

We start by showing the ionization yield curves for the three model molecules in Figs. 3–5. Each figure presents both single ionization (SI) and double ionization (DI) yields. Circles correspond to the parallel configuration  $(V_{\parallel})$ , while filled triangles represent the perpendicular configuration  $(V_{\perp 2})$ . The choice of different frequencies  $\omega$  is motivated by classical scaling (see Table II).

The characteristic knee structure in the DI yield curve is visible in all three cases, indicating the presence of NSDI channel. In each case, the position of the knee correlates well with the saturation of the SI yield, as expected. The observed shift of the knee onset towards lower field amplitudes when moving from  $N_2$  to  $O_2$  and then to  $S_2$  reflects the decreasing ionization potential across this sequence. This trend is not attributed to the change in frequency [27].

When comparing the yield curves, the different configurations do not lead to visible differences in the case of  $N_2$  and  $O_2$  (see Figs. 3 and 4), whereas for  $S_2$  (Fig. 5) the difference is clearly pronounced. Several factors may contribute to the observed discrepancy between  $N_2$  (or  $O_2$ ) and  $S_2$ . One possible explanation lies in the actual differences in ionization energies between the two configurations for the same molecular species. For  $S_2$ , these differences are  $\Delta E_I^+ = 1.2$  eV and  $\Delta E_I^{2+} = 1.4$  eV. However, for  $N_2$ , the differences are smaller ( $\Delta E_I^+ = 0.8$  eV and  $\Delta E_I^{2+} = 0.7$  eV) and the ionization yields for different configurations are virtually identical (compare Figs. 3

and 5).

Another contributing factor is the difference in the cutoff parameter  $\epsilon$  between the two alignments. For  $S_2$ , the difference is relatively large ( $\Delta \epsilon = 1.4$ ), while for  $O_2$ and  $N_2$  it is smaller ( $\Delta \epsilon = 0.4$  in both cases). In all three molecules,  $\epsilon$  is larger for the parallel configuration than for the perpendicular one. As a result, the electron–electron repulsion term in  $V_{\parallel}$  is shallower than in  $V_{\perp 2}$ , leading to a reduction in electron–electron interaction. Since NSDI is rooted in electron-electron correlations, it strongly depends on this interaction term. Therefore, one can expect the DI yield for  $V_{\parallel}$  to be lower than for  $V_{\perp 2}$  in the NSDI regime. This effect should be particularly pronounced for S<sub>2</sub>, and indeed, Fig. 5 shows a smaller DI yield for  $V_{\parallel}$ . We thus consider this modelspecific effect to be the most likely explanation for the behavior of the  $S_2$  ionization yields.

Overall, the results indicate that ionization yields vary little with molecular orientation. This is consistent with the findings of Prauzner-Bechcicki  $et\ al.$  in the classical model analysis [73]. However, experimental results by Zeidler  $et\ al.$  [43] show that 30% more  $N_2^{2+}$  ions and 19% more  $N_2^{+}$  ions are produced for parallel alignment compared to perpendicular alignment. Moreover, S-matrix calculations suggest that the electronic structure of the molecular orbital influences ionization [49, 87]. This indicates that the symmetry of the molecular orbital relative to the laser polarization axis may play a significant role. While this observation could explain the discrepancy between experimental data and our numerical results, a full test of this hypothesis is, as noted earlier, beyond the predictive power of the present model.

To further compare the studied molecular species, we apply the classical scaling described in the previous section. As an example, we first show a comparison of ionization yields for the perpendicular orientation  $(V_{\perp 2})$  between N<sub>2</sub> and O<sub>2</sub> in Fig. 6, and for the parallel orientation  $(V_{\parallel})$  between N<sub>2</sub> and S<sub>2</sub> in Fig. 7. In both cases, a remarkably good agreement in the global trend is observed, highlighting once again the model's limited ability to distinguish between molecular species.

A similar behavior is found for all other molecule pairs with the same orientation, except for those involving the  $V_{\perp 2}$  potential of  $S_2$ . For instance, Fig. 8 illustrates the differences in this case for  $N_2$  and  $S_2$ . Again, we attribute the discrepancy to the strong reduction of electron–electron repulsion caused by the choice of the cut-off parameter  $\epsilon$ .

Eremina et al. argued in [42] that SI depends on the molecular structure. Since SI is the first step in the rescattering mechanism [3, 4], they also expected the molecular symmetry to influence the NSDI process. Indeed, their measurements confirmed such a dependence [42]. Similarly, Guo et al. reported a significantly reduced DI rate for  $O_2$  and attributed it to the molecular structure of the molecule [38].

While we again reach the limits of the predictive power of the present model, one experimental suggestion may be

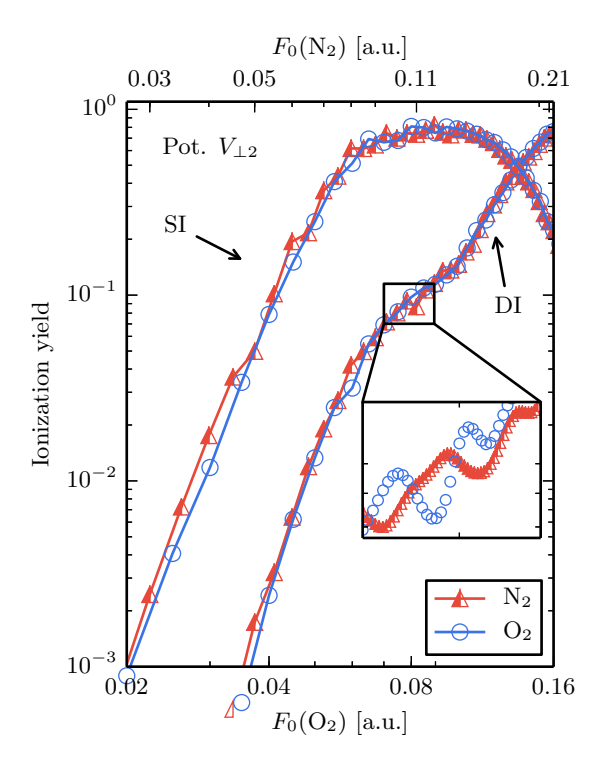


FIG. 6. (Color online) Comparison of the single ionization (SI) and double ionization (DI) yields of potential  $V_{\perp 2}$  of  $N_2$  ( $\omega=0.075$  a.u.) and  $O_2$  ( $\omega=0.06$  a.u.). The peak field amplitudes  $F_0$  for  $N_2$  (top axis) have been rescaled according to Eq. (21).

formulated: the field amplitudes and frequencies should be adapted according to classical scaling. If differences in ionization yields persist under such conditions, this would indicate that the molecular structure indeed plays a significant role in the DI process.

A detailed analysis of the DI yield curves reveals the presence of small-scale, non-monotonic variations, including local extrema. These features were initially identified during a coarse-grained scan along the field amplitude axis and are highlighted in the inset of Fig. 6. The inset presents a segment of the yield curves obtained with finer steps in  $F_0$ , ruling out the possibility that the observed extrema are numerical artifacts. Similar structures are visible in Fig. 3 for  $V_{\parallel}$  near  $F_0 \approx 0.09$  a.u. and for  $V_{\perp 2}$  near  $F_0 \approx 0.11$  a.u., as well as in Fig. 5 for  $V_{\perp 2}$ near  $F_0 \approx 0.05$  a.u. Increasing the resolution of the field amplitude scan by reducing the step size  $\Delta F_0$  reveals even more of these genuine dynamical features. These structures are not restricted to a particular molecule or potential and can be observed across different frequencies, albeit at different values of  $F_0$ . Furthermore, extrema visible in the DI yield for  $V_{\parallel}$  often have counterparts at similar  $F_0$  values in the DI yield for  $V_{\perp 2}$ .

Panfili et al. [88] identified similar local extrema in the ionization yield of a model helium atom and attributed them to multiphoton resonances between the ground state and low-lying bound states. In their simula-

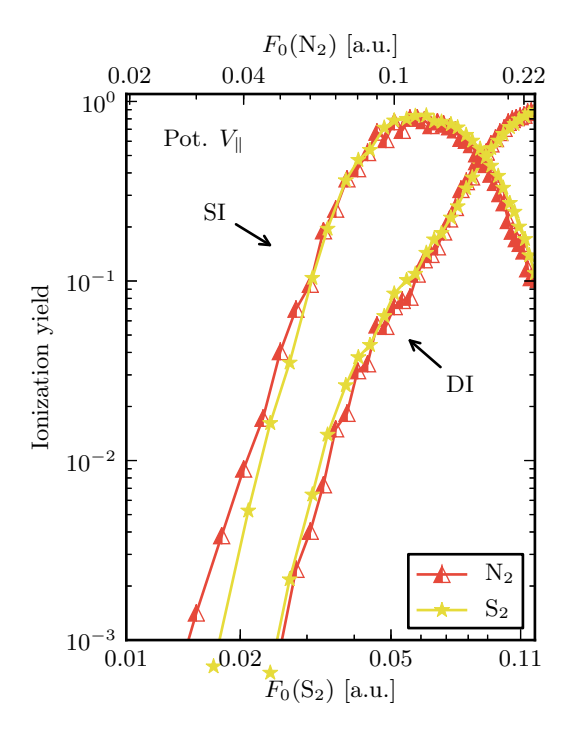


FIG. 7. (Color online) Comparison of the single ionization (SI) and double ionization (DI) yields of potential  $V_{\parallel}$  of N<sub>2</sub> ( $\omega=0.075$  a.u.) and S<sub>2</sub> ( $\omega=0.045$  a.u.). The peak field amplitudes  $F_0$  for N<sub>2</sub> (top axis) have been rescaled according to Eq. (21).

tions, they used a sine pulse with a trapezoidal envelope and found that increasing the number of field cycles  $n_c$  enhanced the amplitude of the maxima.

To test this behavior, we repeated our simulations using a trapezoidal pulse shape and verified that the extrema become more pronounced with increasing pulse duration. This is illustrated in Fig. 9 for the case of  $S_2$  and potential  $V_{\perp 2}$ . For longer pulses, the peaks can be associated with resonances among eigenstates of the periodically driven system, i.e., its Floquet states. Similar phenomena have been observed in microwave ionization of atomic systems [89, 90], where they were directly linked to Floquet resonances. Although we do not explicitly construct Floquet states in the present model, the stabilization of the ionization yield with increasing pulse duration supports the interpretation in terms of resonance effects.

## B. Momentum distributions

Having identified the limitations of the analyzed model, we decided not to study the dependence of momentum distributions on molecular orientation or species. However, in Fig. 10, we present both the two-electron momentum distribution and the ion momentum distribution for  $O_2$  in the parallel configuration, at  $F_0=0.06$  a.u. and  $\omega=0.06$  a.u., averaged over eight

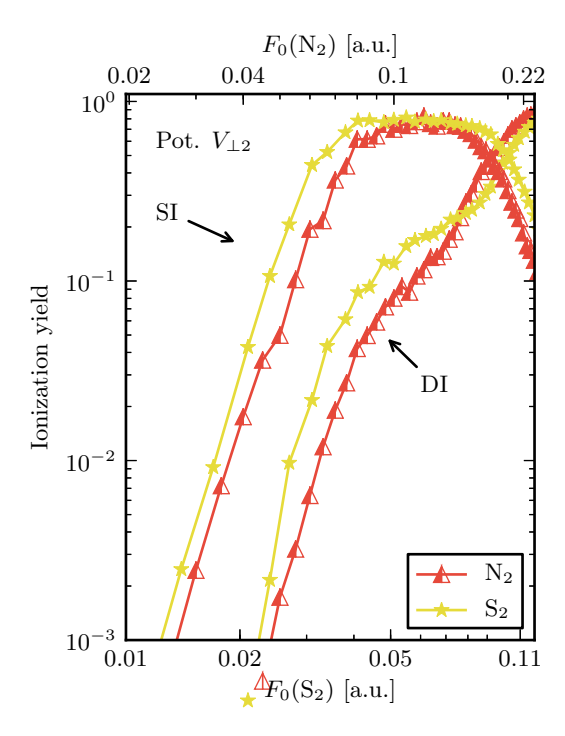


FIG. 8. (Color online) Comparison of the single ionization (SI) and double ionization (DI) yields of potential  $V_{\perp 2}$  of  $N_2$  ( $\omega = 0.075$  a.u.) and  $S_2$  ( $\omega = 0.045$  a.u.). The peak field amplitudes  $F_0$  for  $N_2$  (top axis) have been rescaled according to Eq. (21).

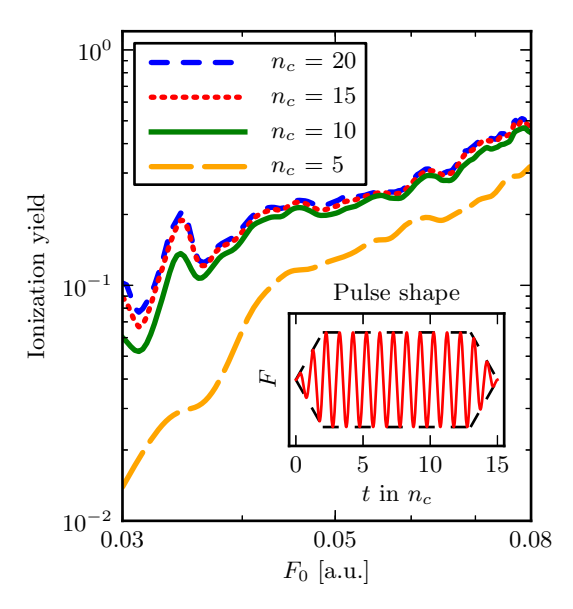


FIG. 9. (Color online) Resonances for different numbers of field cycles  $n_c$  in the knee region of S<sub>2</sub> potential  $V_{\perp 2}$  at  $\omega = 0.06$  a.u. An example for  $n_c = 15$  of the used laser pulse with trapezoidal envelope and two cycle turn-on time is displayed as an inset.

carrier-envelope phases. These distributions correspond to experimentally accessible observables: two-electron

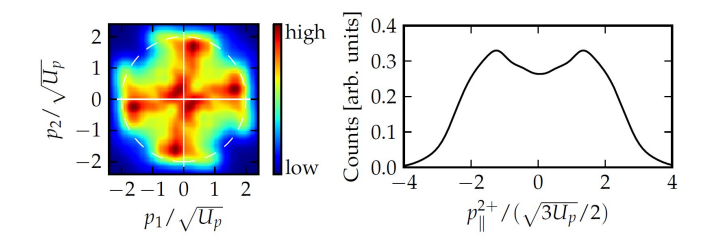


FIG. 10. (Color online) Two-electron momentum distribution (left) and ion momentum distribution (right) for  $O_2$  in the parallel configuration, at  $F_0=0.06$  a.u. and  $\omega=0.06$  a.u., averaged over eight carrier-envelope phases. The dashed circle indicates the maximum momentum that electrons can classically gain in the field.

momentum distributions and ion momentum distributions measured along the laser polarization axis.

The obtained results, although averaged over only eight phases, closely resemble those reported by Kübel et al. in [56]. In their work, Kübel et al. compared the  $N_2$  molecule with its atomic counterpart, the Ar atom, and discussed similarities and differences in the two-electron momentum distributions. Both species exhibit asymmetric energy sharing between the escaping electrons, which is associated with the RESI mechanism. In the case of  $N_2$ , the distributions also show a contribution from low-energy anticorrelated electrons, which leads to a flat-top structure in the ion momentum distribution. This contribution was attributed to the presence of excited states in  $N_2^+$  [56].

A similar effect is visible in both the two-electron and ion momentum distributions obtained with our model (see Fig. 10). We chose to present results for  $O_2$  to emphasize the model's inherent limitation in distinguishing between different molecular species. Despite this limitation, it is noteworthy that the obtained distributions reproduce the experimental results remarkably well.

There is a difference in the symmetry of the valence orbital between  $N_2$  and  $O_2$ :  $N_2$  has a  $\sigma_g$  bonding symmetry, while  $O_2$  has a  $\pi_g$  antibonding symmetry. The acquired results suggest that the introduced model is well suited to study systems with  $\sigma$ -type symmetry, such as  $N_2$ , whereas its application to systems with other orbital symmetries may require further extension. Exploring how to incorporate the molecular orbital symmetry degree of freedom into the restricted-geometry framework could be a promising direction for future research.

#### V. CONCLUSIONS

We introduced a (1+1)-dimensional quantum model capable of describing non-sequential double ionization (NSDI) in homonuclear diatomic molecules. The model is a straightforward extension of the restricted-geometry Eckhardt–Sacha approach previously used for atoms. We

thoroughly discussed the rationale behind this framework and clearly stated its assumptions and limitations. Wherever possible, we pointed out conceivable extensions of the approach. The numerical methodology was also outlined.

Within the proposed model, we analyzed ionization yield curves for two extreme molecular orientations and three different species. The results confirmed the model's limitations, while simultaneously demonstrating its ability to capture subtle dynamical effects, such as the resonances observed in the DI yield curves. By applying classical scaling, we were able to map the yield curves of different molecules onto each other. When such scaling is applied to experimental data, any remaining differences in the yields may indicate quantum effects, resonances being one such example observed in our simulations.

Finally, the comparison between the obtained two-

electron and ion momentum distributions and existing experimental data shows that, despite its simplifying assumptions and clear limitations, the restricted-geometry quantum model is suitable for studying NSDI in diatomic molecules with  $\sigma$ -type symmetry.

#### ACKNOWLEDGMENTS

The L.C.B., J.H.T and J.S.P.-B. acknowledge the late Bruno Eckhardt with whom we had the honor of working. The above work was initiated and stimulated by him.

D.K.E. and M.O. gratefully acknowledge Polish high-performance computing infrastructure PLGrid (HPC Center: ACK Cyfronet AGH) for providing computer facilities and support within computational grant no. PLG/2025/018418.

- M. Lewenstein, P. Balcou, M. Y. Ivanov, A. L'Huillier, and P. B. Corkum, Theory of high-harmonic generation by low-frequency laser fields, Phys. Rev. A 49, 2117 (1994).
- [2] K. Amini, J. Biegert, F. Calegari, A. Chacón, M. F. Ciappina, A. Dauphin, D. K. Efimov, C. Figueira de Morisson Faria, K. Giergiel, P. Gniewek, A. S. Landsman, M. Lesiuk, M. Mandrysz, A. S. Maxwell, R. Moszyński, L. Ortmann, J. Antonio Pérez-Hernández, A. Picón, E. Pisanty, J. Prauzner-Bechcicki, K. Sacha, N. Suárez, A. Zaïr, J. Zakrzewski, and M. Lewenstein, Symphony on strong field approximation, Rep. Prog. Phys. 82, 116001 (2019).
- [3] P. B. Corkum, Plasma perspective on strong field multiphoton ionization, Phys. Rev. Lett. 71, 1994 (1993).
- [4] K. C. Kulander, K. J. Schafer, and J. Krause, Dynamics of short-pulse excitation, ionization and harmonic conversion, in Super-Intense Laser-Atom Physics, NATO Advanced Science Institutes Series, Series B, Physics, Vol. 316, edited by B. Piraux, A. L'Huillier, and K. Rzazewski (NATO, Sci Affairs Div, 1993) p. 95, proceedings of NATO Advanced Research Workshop on SILAP (Super-Intense Laser-Atom Physics), Han-Sur-Lesse, Belgium, Jan 08-14, 1993.
- [5] B. Eckhardt and K. Sacha, Classical analysis of correlated multiple ionization in strong fields, Physica Scripta 2001, 185 (2001).
- [6] B. Eckhardt and K. Sacha, Wannier threshold law for two-electron escape in the presence of an external electric field, Europhys. Lett. 56, 651 (2001).
- [7] K. Sacha and B. Eckhardt, Pathways to double ionization of atoms in strong fields, Phys. Rev. A 63, 043414 (2001).
- [8] K. Sacha and B. Eckhardt, Nonsequential triple ionization in strong fields, Phys. Rev. A 64, 053401 (2001).
- [9] K. Sacha and B. Eckhardt, Pathways to non-sequential multiple ionization in strong laser fields, J. Phys. B: At. Mol. Opt. Phys. 36, 3923 (2003).
- [10] B. Eckhardt and K. Sacha, Classical threshold behaviour in a (1+1)-dimensional model for double ionization in strong fields, J. Phys. B: At. Mol. Opt. Phys. 39, 3865 (2006).

- [11] J. S. Prauzner-Bechcicki, K. Sacha, B. Eckhardt, and J. Zakrzewski, Time-resolved quantum dynamics of double ionization in strong laser fields, Phys. Rev. Lett. 98, 203002 (2007).
- [12] J. S. Prauzner-Bechcicki, K. Sacha, B. Eckhardt, and J. Zakrzewski, Quantum model for double ionization of atoms in strong laser fields, Phys. Rev. A 78, 013419 (2008).
- [13] A. L'Huillier, L. A. Lompre, G. Mainfray, and C. Manus, Multiply charged ions formed by multiphoton absorption processes in the continuum, Phys. Rev. Lett. 48, 1814 (1982).
- [14] A. L'Huillier, L. A. Lompré, G. Mainfray, and C. Manus, Multiply charged ions induced by multiphoton absorption in rare gases at 0.53  $\mu$ m, Phys. Rev. A **27**, 2503 (1983).
- [15] B. Walker, B. Sheehy, L. F. DiMauro, P. Agostini, K. J. Schafer, and K. C. Kulander, Precision measurement of strong field double ionization of helium, Phys. Rev. Lett. 73, 1227 (1994).
- [16] S. Larochelle, A. Talebpour, and S. L. Chin, Non-sequential multiple ionization of rare gas atoms in a Ti:sapphire laser field, J. Phys. B: At. Mol. Opt. Phys. 31, 1201 (1998).
- [17] T. Weber, M. Weckenbrock, A. Staudte, L. Spielberger, O. Jagutzki, V. Mergel, F. Afaneh, G. Urbasch, M. Vollmer, H. Giessen, and R. Dörner, Recoil-ion momentum distributions for single and double ionization of helium in strong laser fields, Phys. Rev. Lett. 84, 443 (2000).
- [18] R. Moshammer, B. Feuerstein, W. Schmitt, A. Dorn, C. D. Schröter, J. Ullrich, H. Rottke, C. Trump, M. Wittmann, G. Korn, K. Hoffmann, and W. Sandner, Momentum distributions of Ne<sup>n+</sup> ions created by an intense ultrashort laser pulse, Phys. Rev. Lett. 84, 447 (2000).
- [19] T. Weber, H. Giessen, M. Weckenbrock, G. Urbasch, A. Staudte, L. Spielberger, O. Jagutzki, V. Mergel, M. Vollmer, and R. Dörner, Correlated electron emission in multiphoton double ionization, Nature 405, 658 (2000).

- [20] A. Staudte, C. Ruiz, M. Schöffler, S. Schössler, D. Zeidler, T. Weber, M. Meckel, D. M. Villeneuve, P. B. Corkum, A. Becker, and R. Dörner, Binary and recoil collisions in strong field double ionization of helium, Phys. Rev. Lett. 99, 263002 (2007).
- [21] A. Rudenko, V. L. B. de Jesus, T. Ergler, K. Zrost, B. Feuerstein, C. D. Schröter, R. Moshammer, and J. Ullrich, Correlated two-electron momentum spectra for strong-field nonsequential double ionization of He at 800 nm, Phys. Rev. Lett. 99, 263003 (2007).
- [22] J. S. Prauzner-Bechcicki, K. Sacha, B. Eckhardt, and J. Zakrzewski, Nonsequential double ionization of atoms in strong laser pulses, Acta Phys. Pol. A 112, 699 (2007).
- [23] B. Eckhardt, J. S. Prauzner-Bechcicki, K. Sacha, and J. Zakrzewski, Suppression of correlated electron escape in double ionization in strong laser fields, Phys. Rev. A 77, 015402 (2008).
- [24] B. Eckhardt, J. Prauzner-Bechcicki, K. Sacha, and J. Zakrzewski, Momentum distributions after double ionization, Chaos 18, 041110 (2008).
- [25] B. Eckhardt, J. S. Prauzner-Bechcicki, K. Sacha, and J. Zakrzewski, Phase effects in double ionization by strong short pulses, Chem. Phys. 370, 168 (2010).
- [26] H. Jiang, M. Mandrysz, A. Sanchez, J. Dura, T. Steinle, J. S. Prauzner-Bechcicki, J. Zakrzewski, M. Lewenstein, F. He, J. Biegert, and M. F. Ciappina, Pulse length effects in long wavelength driven non-sequential double ionization, New J. Phys. 25, 033002 (2023).
- [27] J. H. Thiede and J. S. Prauzner-Bechcicki, Frequency dependence of nonsequential double ionization of atoms in strong laser fields, Phys. Rev. A 110, 053105 (2024).
- [28] D. K. Efimov, A. Maksymov, J. S. Prauzner-Bechcicki, J. H. Thiede, B. Eckhardt, A. Chacón, M. Lewenstein, and J. Zakrzewski, Restricted-space ab initio models for double ionization by strong laser pulses, Phys. Rev. A 98, 013405 (2018).
- [29] J. H. Thiede, B. Eckhardt, D. K. Efimov, J. S. Prauzner-Bechcicki, and J. Zakrzewski, Ab initio study of time-dependent dynamics in strong-field triple ionization, Phys. Rev. A 98, 031401 (2018).
- [30] D. K. Efimov, J. S. Prauzner-Bechcicki, J. H. Thiede, B. Eckhardt, and J. Zakrzewski, Double ionization of a three-electron atom: Spin correlation effects, Phys. Rev. A 100, 063408 (2019).
- [31] D. K. Efimov, J. S. Prauzner-Bechcicki, and J. Zakrzewski, Strong-field ionization of atoms with p<sup>3</sup> valence shell: Two versus three active electrons, Phys. Rev. A 101, 063402 (2020).
- [32] J. S. Prauzner-Bechcicki, D. K. Efimov, M. Mandrysz, and J. Zakrzewski, Strong-field triple ionisation of atoms with  $p^3$  valence shell, J. Phys. B: At. Mol. Opt. Phys. **54**, 114001 (2021).
- [33] D. K. Efimov, A. Maksymov, M. Ciappina, J. S. Prauzner-Bechcicki, M. Lewenstein, and J. Zakrzewski, Three-electron correlations in strong laser field ionization, Opt. Express 29, 26526 (2021).
- [34] D. K. Efimov, A. Maksymov, J. Zakrzewski, and J. S. Prauzner-Bechcicki, Strong-field double ionization in a three-electron atom: Momentum-distribution analysis, Phys. Rev. A 108, 033103 (2023).
- [35] D. K. Efimov, G. P. Katsoulis, T. Rozpetkowski, S. Chwałowski, A. Emmanouilidou, and J. S. Prauzner-Bechcicki, Quantum versus semiclassical signatures of correlated triple ionization in dalitz plots, Phys. Rev. A

- **112**, 013111 (2025).
- [36] A. Talebpour, S. Larochelle, and S. L. Chin, Nonsequential ionization of atoms and diatomic molecules in intense laser field, Laser Phys. 7, 851 (1997).
- [37] C. Cornaggia and P. Hering, Laser-induced non-sequential double ionization of small molecules, J. Phys. B: At. Mol. Opt. Phys. 31, L503 (1998).
- [38] C. Guo, M. Li, J. P. Nibarger, and G. N. Gibson, Single and double ionization of diatomic molecules in strong laser fields, Phys. Rev. A 58, R4271 (1998).
- [39] C. Guo, M. Li, J. P. Nibarger, and G. N. Gibson, Nonsequential double ionization of molecular fragments, Phys. Rev. A 61, 033413 (2000).
- [40] A. S. Alnaser, T. Osipov, E. P. Benis, A. Wech, B. Shan, C. L. Cocke, X. M. Tong, and C. D. Lin, Rescattering double ionization of D<sub>2</sub> and H<sub>2</sub> by intense laser pulses, Phys. Rev. Lett. 91, 163002 (2003).
- [41] A. S. Alnaser, S. Voss, X.-M. Tong, C. M. Maharjan, P. Ranitovic, B. Ulrich, T. Osipov, B. Shan, Z. Chang, and C. L. Cocke, Effects of molecular structure on ion disintegration patterns in ionization of O<sub>2</sub> and N<sub>2</sub> by short laser pulses, Phys. Rev. Lett. 93, 113003 (2004).
- [42] E. Eremina, X. Liu, W. Sandner, M. G. Schätzel, A. Dreischuh, G. G. Paulus, H. Walther, R. Moshammer, and J. Ullrich, Influence of molecular structure on double ionization of N<sub>2</sub> and O<sub>2</sub> by high intensity ultrashort laser pulses, Phys. Rev. Lett. 92, 173001 (2004).
- [43] D. Zeidler, A. Staudte, A. B. Bardon, D. M. Villeneuve, R. Dörner, and P. B. Corkum, Controlling attosecond double ionization dynamics via molecular alignment, Phys. Rev. Lett. 95, 203003 (2005).
- [44] D. Zeidler, A. B. Bardon, A. Staudte, D. M. Villeneuve, R. Dörner, and P. B. Corkum, Alignment independence of the instantaneous ionization rate for nitrogen molecules, J. Phys. B: At. Mol. Opt. Phys. 39, L159 (2006).
- [45] J. Chen, J. Fan, Y. Li, and S. P. Yang, Semiclassical theory of molecular nonsequential double ionization, Phys. Rev. A 76, 013418 (2007).
- [46] O. Herrwerth, A. Rudenko, M. Kremer, V. L. B. de Jesus, B. Fischer, G. Gademann, K. Simeonidis, A. Achtelik, T. Ergler, B. Feuerstein, C. D. Schröter, R. Moshammer, and J. Ullrich, Wavelength dependence of sub-laser-cycle few-electron dynamics in strong-field multiple ionization, New Journal of Physics 10, 025007 (2008).
- [47] S. Baier, A. Becker, and L. Plaja, Nonsequential double ionization of the hydrogen molecule: Dependence on molecular alignment, Phys. Rev. A 78, 013409 (2008).
- [48] Q. Liao and P. Lu, Manipulating nonsequential double ionization via alignment of asymmetric molecules, Opt. Express 17, 15550 (2009).
- [49] X.-Y. Jia, W.-D. Li, J. Liu, and J. Chen, Alignment-dependent nonsequential double ionization of N<sub>2</sub> in intense laser fields: The role of different valence orbitals, Phys. Rev. A 80, 053405 (2009).
- [50] F. Mauger, C. Chandre, and T. Uzer, Strong field double ionization of  $\rm H_2$ : Insights from nonlinear dynamics, Chem. Phys. **366**, 64 (2009).
- [51] Z. Wu, C. Wu, X. Liu, Y. Deng, Q. Gong, D. Song, and H. Su, Double ionization of nitrogen from multiple orbitals, The Journal of Physical Chemistry A 114, 6751 (2010).
- [52] C. Huang, Y. Zhou, A. Tong, Q. Liao, W. Hong, and P. Lu, The effect of molecular alignment on correlated

- electron dynamics in nonsequential double ionization, Opt. Express 19, 5627 (2011).
- [53] J. Durá, A. Grün, P. K. Bates, S. M. Teichmann, T. Ergler, A. Senftleben, T. Pflüger, C. D. Schröter, R. Moshammer, J. Ullrich, A. Jaroń-Becker, A. Becker, and J. Biegert, Wavelength dependence of the suppressed ionization of molecules in strong laser fields, The Journal of Physical Chemistry A 116, 2662 (2012).
- [54] Z. Y. Lin, X. Y. Jia, C. L. Wang, Z. L. Hu, H. P. Kang, W. Quan, X. Y. Lai, X. J. Liu, J. Chen, B. Zeng, W. Chu, J. P. Yao, Y. Cheng, and Z. Z. Xu, Ionization suppression of diatomic molecules in an intense midinfrared laser field, Phys. Rev. Lett. 108, 223001 (2012).
- [55] A. Emmanouilidou, C. Lazarou, A. Staudte, and U. Eichmann, Routes to formation of highly excited neutral atoms in the breakup of strongly driven H<sub>2</sub>, Phys. Rev. A 85, 011402 (2012).
- [56] M. Kübel, N. G. Kling, K. J. Betsch, N. Camus, A. Kaldun, U. Kleineberg, I. Ben-Itzhak, R. R. Jones, G. G. Paulus, T. Pfeifer, J. Ullrich, R. Moshammer, M. F. Kling, and B. Bergues, Nonsequential double ionization of n<sub>2</sub> in a near-single-cycle laser pulse, Phys. Rev. A 88, 023418 (2013).
- [57] X.-Y. Jia, D.-H. Fan, W.-D. Li, and J. Chen, Nonsequential double ionization of nonaligned diatomic molecules N<sub>2</sub> and O<sub>2</sub>, Chinese Phys. B 22, 013303 (2013).
- [58] Y. Li, S. P. Yang, J. Chen, and J. Fan, Non-sequential double ionization of diatomic molecules: alignment dependence of electron correlation, J. Phys. B: At. Mol. Opt. Phys. 47, 045601 (2014).
- [59] S. Wang and Y. Chen, Attosecond double-ionization dynamics of aligned H<sub>2</sub>: Two-dimensional quantum simulations, Phys. Rev. A 92, 023418 (2015).
- [60] C. Cheng, P. Vindel-Zandbergen, S. Matsika, and T. Weinacht, Electron correlation in channel-resolved strong-field molecular double ionization, Phys. Rev. A 100, 053405 (2019).
- [61] X. Li, J. Yu, H. Xu, X. Yu, Y. Yang, Z. Wang, P. Ma, C. Wang, F. Guo, Y. Yang, S. Luo, and D. Ding, Multiorbital and excitation effects on dissociative double ionization of CO molecules in strong circularly polarized laser fields, Phys. Rev. A 100, 013415 (2019).
- [62] S. Li, D. Sierra-Costa, M. J. Michie, I. Ben-Itzhak, and M. Dantus, Control of electron recollision and molecular nonsequential double ionization, Communications Physics 3, 35 (2020).
- [63] V. Hanus, S. Kangaparambil, S. Larimian, M. Dorner-Kirchner, X. Xie, M. S. Schöffler, G. G. Paulus, A. Baltuška, A. Staudte, and M. Kitzler-Zeiler, Experimental separation of subcycle ionization bursts in strongfield double ionization of H<sub>2</sub>, Phys. Rev. Lett. 124, 103201 (2020).
- [64] A. J. Howard, C. Cheng, R. Forbes, G. A. McCracken, W. H. Mills, V. Makhija, M. Spanner, T. Weinacht, and P. H. Bucksbaum, Strong-field ionization of water: Nuclear dynamics revealed by varying the pulse duration, Phys. Rev. A 103, 043120 (2021).
- [65] C. Cheng, Z. L. Streeter, A. J. Howard, M. Spanner, R. R. Lucchese, C. W. McCurdy, T. Weinacht, P. H. Bucksbaum, and R. Forbes, Strong-field ionization of water. ii. electronic and nuclear dynamics en route to double ionization, Phys. Rev. A 104, 023108 (2021).
- [66] D. Ren, S. Wang, C. Chen, X. Li, X. Yu, X. Zhao, P. Ma, C. Wang, S. Luo, Y. Chen, and D. Ding, Alignment de-

- pendence of photoelectron momentum distributions for diatomic molecule  $N_2$  in strong elliptical laser fields, J. Phys. B: At. Mol. Opt. Phys. **55**, 175101 (2022).
- [67] C. H. Yuen and C. D. Lin, Density-matrix approach for sequential dissociative double ionization of molecules, Phys. Rev. A 106, 023120 (2022).
- [68] C. H. Yuen and C. D. Lin, Theory of strong-field sequential double ionization of polyatomic molecules, Phys. Rev. A 109, 033108 (2024).
- [69] Y.-W. Jia, C. H. Yuen, W.-Q. Jing, Z.-Y. Zhou, C. D. Lin, and S.-F. Zhao, Improved model for the dissociative sequential double ionization of nitrogen molecules by an intense few-cycle infrared laser pulse, Phys. Rev. A 110, 023112 (2024).
- [70] G. P. Katsoulis, A. Hadjipittas, B. Bergues, M. F. Kling, and A. Emmanouilidou, Slingshot nonsequential double ionization as a gate to anticorrelated two-electron escape, Phys. Rev. Lett. 121, 263203 (2018).
- [71] N. Camus, B. Fischer, M. Kremer, V. Sharma, A. Rudenko, B. Bergues, M. Kübel, N. G. Johnson, M. F. Kling, T. Pfeifer, J. Ullrich, and R. Moshammer, Attosecond correlated dynamics of two electrons passing through a transition state, Phys. Rev. Lett. 108, 073003 (2012).
- [72] V. I. Arnold, Mathematical methods of classical mechanics, Vol. 60 (Springer Science & Business Media, New York, 2013).
- [73] J. S. Prauzner-Bechcicki, K. Sacha, B. Eckhardt, and J. Zakrzewski, Nonsequential double ionization of molecules, Phys. Rev. A 71, 033407 (2005).
- [74] J. S. Prauzner-Bechcicki, K. Sacha, and B. Eckhardt, Nonsequential double ionization of molecules in a strong laser field, Laser Phys. 15, 497 (2005).
- [75] R. Grobe and J. H. Eberly, Photoelectron spectra for a two-electron system in a strong laser field, Phys. Rev. Lett. 68, 2905 (1992).
- [76] R. Grobe and J. H. Eberly, One-dimensional model of a negative ion and its interaction with laser fields, Phys. Rev. A 48, 4664 (1993).
- [77] D. Bauer, Two-dimensional, two-electron model atom in a laser pulse: Exact treatment, single-active-electron analysis, time-dependent density-functional theory, classical calculations, and nonsequential ionization, Phys. Rev. A 56, 3028 (1997).
- [78] D. G. Lappas and R. van Leeuwen, Electron correlation effects in the double ionization of he, J. Phys. B: At., Mol. Opt. Phys. 31, L249 (1998).
- [79] W.-C. Liu, J. H. Eberly, S. L. Haan, and R. Grobe, Correlation effects in two-electron model atoms in intense laser fields, Phys. Rev. Lett. 83, 520 (1999).
- [80] M. Lein, E. K. U. Gross, and V. Engel, Intense-field double ionization of helium: Identifying the mechanism, Phys. Rev. Lett. 85, 4707 (2000).
- [81] C. Ruiz, L. Plaja, L. Roso, and A. Becker, Ab initio calculation of the double ionization of helium in a few-cycle laser pulse beyond the one-dimensional approximation, Phys. Rev. Lett. 96, 053001 (2006).
- [82] K. P. Huber and G. Herzberg, Constants of diatomic molecules, in NIST Chemistry WebBook, NIST Standard Reference Database Number 69, edited by P. J. Linstrom and W. G. Mallard (National Institute of Standards and Technology, Gaithersburg, MD, http://webbook.nist.gov, retrieved April 28, 2014) Chap. Constants of Diatomic Molecules.
- [83] D. R. Lide, ed., CRC Handbook of Chemistry and

- Physics, 89th ed. (CRC Press, Boca Raton, FL, 2008).
- [84] M. D. Feit, J. A. Fleck, and A. Steiger, Solution of the schrödinger equation by a spectral method, Journal of Computational Physics 47, 412 (1982).
- [85] G. Dattoli, P. L. Ottaviani, A. Segreto, and T. A., Symmetric-split-operator techniques and finite-difference methods for the solution of classical and quantum evolution problems, Nouv. Cim. B 111, 825 (1996).
- [86] D. Dundas, K. T. Taylor, J. S. Parker, and E. S. Smyth, Double-ionization dynamics of laser-driven helium, J. Phys. B: At. Mol. Opt. Phys. 32, L231 (1999).
- [87] C. Figueira de Morisson Faria, T. Shaaran, X. Liu, and

- W. Yang, Quantum interference in laser-induced nonsequential double ionization in diatomic molecules: Role of alignment and orbital symmetry, Phys. Rev. A **78**, 043407 (2008).
- [88] R. Panfili and W.-C. Liu, Resonances in the doubleionization signal of two-electron model atoms, Phys. Rev. A 67, 043402 (2003).
- [89] R. Blümel and U. Smilansky, Localization of floquet states in the rf excitation of rydberg atoms, Phys. Rev. Lett. 58, 2531 (1987).
- [90] P. M. Koch and K. A. H. van Leeuwen, The importance of resonances in microwave "ionization" of excited hydrogen atoms, Phys. Rep. 255, 289 (1995).